JOURNAL OF MATERIALS SCIENCE 29 (1994) 5357–5366

Evolution of microstructure and local thermal conditions during directional solidification of A356-SiC particle composites

P. K. ROHATGI, K. PASCIAK, C. S. NARENDRANATH
Department of Materials, University of Wisconsin-Milwaukee, Milwaukee, WI 53211, USA

S. RAY
Department of Metallurgical Engineering, University of Roorkee, Roorkee, Uttar Pradesh, 247667, India

A. SACHDEV
General Motors Research Laboratories, Warren, Michigan, MI 48090

Solidification microstructures of aluminium silicon alloy (A-356) containing 0, 10, 15 and 20 vol% silicon carbide particles formed during directional solidification from a chill have been studied and compared with the structures obtained during solidification of the base alloy under similar mould and chill conditions. Columnar dendritic structure was observed during solidification of the base alloy at all distances from the chill. In the case of composites, the presence of silicon carbide particles disturbs the orderly aligned arrangement of dendrites observed in the base alloy, under similar solidification conditions, except near the chill surface where a particle-free zone is observed due to probable pushing of particles by the macroscopic solidification front with cell spacings finer than the particle size. During the entire range of solidification conditions studied in this work, the silicon carbide particles are pushed by growing dendrites of α-aluminium into the last freezing eutectic liquid. The observations on pushing of silicon carbide particles have been examined in relation to existing models on particle pushing by planar solidification fronts. Even in the regions away from the chill, where silicon carbide particles are present, there are large regions covering several dendrite arm spacings where there are no particles representing another form of macrosegregation of particles. It is observed that the secondary dendrite arm spacings (DAS) of α-aluminium are related to cooling rate by an equation $DAS = b(T)^n$ for the base alloy as well as for the composite. The coefficient b is generally higher for composites than for base alloy, and it is found to be a function of particle content. The value of n for the composite is close to the value of the base alloy and is not significantly influenced by the presence of particles. Cooling rate, temperature gradients and the rate of advancement of the solidification front have been experimentally measured for the base alloy as well as for the composites during unidirectional solidification. The study indicates that the presence of particles themselves alters the cooling rates, temperature gradients and growth rate of the macroscopic solidification front under identical thermal surroundings during solidification. The possible influences of these alterations in growth condition on the solidification microstructure due to the presence of particles are discussed together with the other possible direct influences of particles on dendritic growth of aluminium–silicon alloys.

1. Introduction

Of the alternate methods available to produce components of metal matrix composites (MMCs), casting processes are attractive because they are economical and have the capability of producing near net-shaped parts. In recent years, casting methods have been used to manufacture a wide range of engineering metal matrix composite components [1–3], particularly of aluminium alloy–silicon carbide particle composites by casting molten metal–ceramic particle composite slurries [4]. The properties of cast aluminium alloy–silicon carbide particle composites strongly depend on the solidification microstructure which, in turn, depends upon the melting and casting procedures. During solidification, cooling rates, temperature gradients, and growth rates have a profound influence on evolution of microstructural features of cast composites, including the particle distribution and the dendritic structure, both of which influence the properties of cast composites.

It has been experimentally observed that generally the α-aluminium phase does not nucleate on the sil-

0022–2461

icon carbide particle surface during solidification of aluminium alloy–silicon carbide composites. Wettability of the silicon carbide surface by molten aluminium alloy is considered to be poor. It has been observed that α-aluminium dendrites which nucleate away from the particles also push the dispersed particles during their growth, causing the particles to be segregated in the interdendritic regions which freeze during the last stages of solidification [5]. There are several models in the literature on interactions between growing planar solid–liquid interfaces and particles which predict conditions under which the particles will be pushed.

Limited information is available on the solidification structure of fibre- and particle-reinforced aluminium alloys [6–8]. Generally, existing knowledge relates to comparing the microstructural features of cast structures in base alloys and composites when they are poured and solidified under identical thermal conditions. Recently, Rohatgi *et al.* [5], Suery and Lajay [9], McCoy and Wawner [10] and Lloyd [11] have related cast microstructures in Al–SiC composites to solidification phenomena. However, these studies have not measured the changes in cooling rates and temperature gradients in the presence of ceramic particles, and their influence on the evolution of the microstructure. The correlations between the cooling rates, temperature gradients, velocity of the solidification front, dendrite arm spacing and particle distribution in Al–SiC composite alloys require further investigation. It is important to understand the influence of particles on the temperature gradients and growth rates under identical mould conditions, together with the direct influence of particles on growing dendrites.

The object of this work was to measure the influence of particles on the cooling rates, temperature gradients and macroscopic growth rate of the solidification front for the composite, and to understand the observed solidification microstructures in the monolithic aluminium silicon alloy and the base alloy containing 0–20 vol % silicon carbide during unidirectional solidification. An attempt has been made to relate experimentally measured temperature gradients, rate of bulk movement of solidification front and cooling rates to dendritic structure including dendrites arm spacing and particle distribution.

2. Experimental procedure

2.1. Melting

Aluminium alloy silicon carbide composite ingots supplied by Duralcan were melted in a resistance furnace. The compositions of the base alloy and the volume fractions of silicon carbide in different composites investigated in this study are given in Table I. The pouring temperature was measured using chromel–alumel thermocouples and the measured temperatures were controlled to within 10 °C. A blanket of argon gas was used over the crucible throughout the melting process to minimize oxidation and the resulting oxide inclusions in the cast composite.

2.2. Directional solidification

The experimental apparatus used for this purpose is shown in Fig. 1. Directional solidification was obtained by placing water-cooled copper chill at the bottom of the insulating mould in direct contact with the liquid metal. Heat was extracted unidirectionally, perpendicular to the copper chill face in contact with the melt when the alloy was poured on the copper chill in the insulating ceramic mould, maintained at a temperature of 585 °C, close to the eutectic temperature of the alloy. The moulds used in these experiments are highly insulating moulds made out of aluminosilicate fibres. In addition, these moulds are heated to 585 °C before pouring the metal. In view of this, it is expected that there was negligible heat flow in the lateral direction. Hence, heat is expected to flow unidirectionally, perpendicular to the chill. The pouring temperature of the metal was maintained at 720 °C in all the heats.

Four chromel–alumel thermocouples indicated by TC_1, TC_2, TC_3, and TC_4 in Fig. 1, were located at 12 mm intervals from the chill surface to record the temperature at these locations as a function of time. Strip chart recorders were used to record the variation

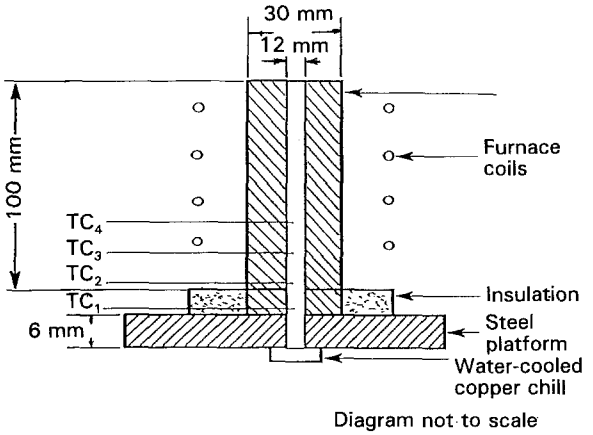

Figure 1 Schematic diagram showing experimental apparatus.

TABLE I Composition of the base alloy and the composites investigated in this study

SiC (vol %)	Alloying elements (wt %)								
	Si	Fe	Cu	Mn	Mg	Cr	Zn	Ti	V
0	7	< 0.2	< 0.2	–	0.35	–	< 0.1	–	–
10	6.9	0.11	0.002	0.005	0.35	0	0.13	0.15	0
15	6.95	0.08	0.01	0.1	0.42	0	0	0.11	0.15
20	7.2	0.15	0.01	0.1	0.40	0.1	0.1	0.15	0.12

in temperature with time during the solidification process.

2.3. Experimental measurements

Temperature versus time curves obtained by different thermocouples, were used for determining the temperature profiles, and for calculating the cooling rates, temperature gradients, and growth rates, at different distances from the chill surface. Cooling rates were calculated from the slopes of the recorded time–temperature curves at the liquidus temperature. The temperature gradient ahead of the solidification front was calculated from the measured temperature profiles. The bulk movement of solidification front, termed the macroscopic growth rate, R, was calculated by dividing the distance between each thermocouple by the time taken for respective thermocouples to reach the liquidus temperature. The time taken for each thermocouple to reach the liquidus temperature was determined from the recorded cooling curves.

2.4. Microstructural analysis

Samples for microstructural analysis were taken from locations near the thermocouple, and were prepared using standard metallographic procedures. Measurements of secondary dendrite arm spacing were carried out after taking several micrographs at higher magnifications at several locations of the unidirectionally solidified sample.

3. Results and discussions

3.1. Temperature gradient

Fig. 2 shows temperature gradients in the melts containing 0, 10, 15 and 20 vol % silicon carbide particles, plotted against distance through which the solid–liquid interface has moved away from the chill. The dendritic solidification front encounters a higher temperature gradient near the chill, but away from the chill, the dendritic solidification takes place under relatively lower temperature gradients. However, it should be noted from Fig. 2 that for similar processing conditions, solidification takes place at all given casting locations (distance from the chill) at a lower temperature gradient in all the composite alloys, than that for the corresponding base alloy. The presence of particles is expected to change the total latent heat to be released and extracted per unit volume of the alloy; the specific heat, conductivity and overall thermophysical properties of the alloy are also changed and, therefore, the temperature profiles and gradients are influenced under identical mould conditions.

3.2. Cooling rate

Fig. 3 shows the variation of cooling rate at the liquidus temperature with distance from the chill for both the base alloy and composites. At any particular location, the cooling rate does not significantly change with particle content in the base alloy. This phenomenon is surprising because the temperature gradient is

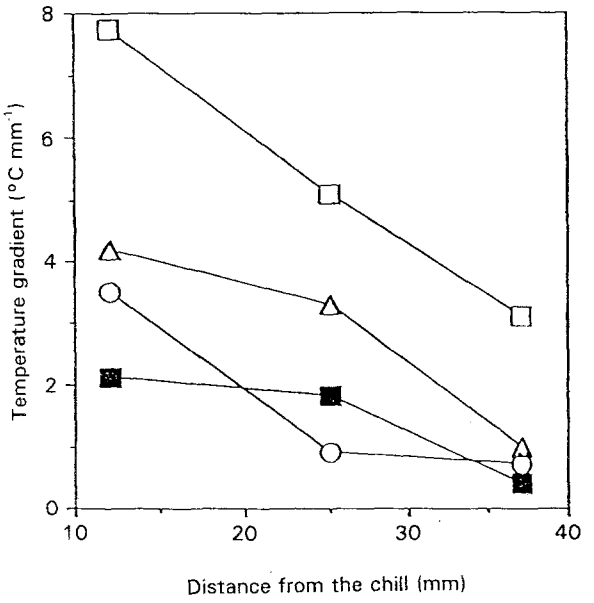

Figure 2 Variation in temperature gradients as a function of distance from the chill. Vol % SiC: (□) 0, (■) 10, (○) 15, (△) 20.

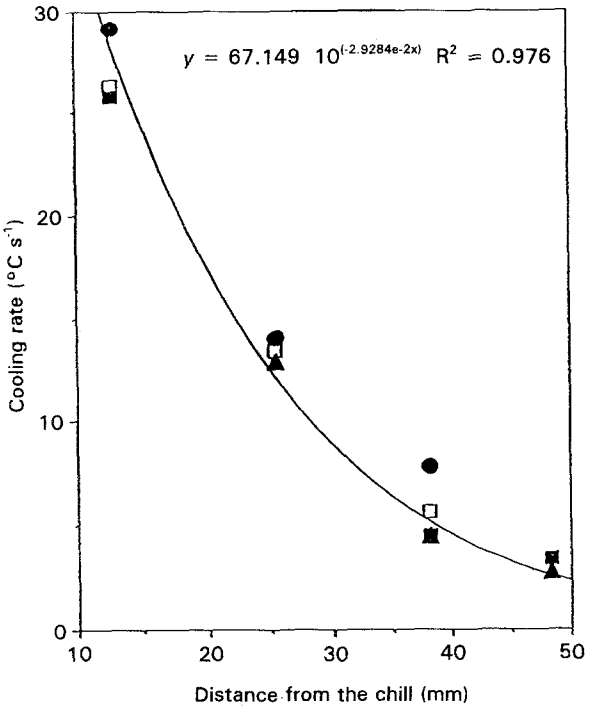

Figure 3 Variation of measured cooling rate as a function of distance from the chill. Vol % SiC: (□) 0, (■) 10, (●) 15, (▲) 20.

lower at higher particle contents, in particular near the chill surface and the average thermal conductivity changes with the particle content. The heat flux at different locations should therefore decrease during solidification of the melt containing particles. However, the heat flux required to maintain a given cooling rate at different cooling locations is also likely to decrease with an increase in particle content because of a decrease in the evolution of latent heat per unit volume of the composite melt, thus not influencing the cooling rate significantly, as observed in Fig. 3.

3.3. Growth rate

Fig. 4 shows that the rate of advancement of the macroscopic solidification front decreases with increasing distance from the chill, and that the growth rate near the chill is lower for alloys containing larger amounts of silicon carbide particles; however, these rates of advancement of solidification fronts are quite close to one another, farther away from the chill, for the base alloy and all the composites studied in the paper.

3.4. Microstructure

Figs 5 and 6 show typical micrographs at various distances from the chill for the base alloy, and the composite containing 20 vol % silicon carbide, respectively. The microstructures in Fig. 5 reveal that in the base alloy columnar dendritic structure persists beyond 50 mm from the chill, while in the composite (Fig. 6), the columnar structure is significantly disturbed beyond the position of the first thermocouple (12 mm). It also appears that the amount of eutectic increases with increasing distance from the chill in both the base alloy and the composite. (The aluminium–silicon–silicon carbide composite used in the present study is a commercial grade composite supplied by Duralcan. Hence, the alloy may contain some modifiers such as sodium or strontium. Very small amounts of these modifiers may remain in the melt after remelting. Their presence is not taken into consideration while analysing the microstructure.) Closer to the chill surface only, secondary dendrite arms are visible in the base alloy, and at distances greater than 25 mm from the chill, tertiary dendrite arms are also observed.

In the composite alloy, containing 20 vol % silicon carbide, as seen from Fig. 6a–d, it may be noted that near the chill a typical chill-cast structure of columnar dendrites was observed where there were no particles present. It appears that the particles have been macroscopically pushed upwards by the closely spaced array of columnar dendrites growing upwards from the chill in this region, where the cell spacing is smaller than the particle size making entrapment difficult in the cell boundaries. This observation suggests that in rapidly solidified aluminium–silicon carbide castings there will be a particle-free region near the outer surface due to macroscopic pushing of the particles. This phenomenon occurs when the dendrite spacing is much smaller compared to the dispersoid size. Similar observations have been made by Wu *et al.* [12]. In addition to the vertical pushing of particles by the dendrites near the chill, particle pushing is also observed in the present investigation at greater distance from the chill.

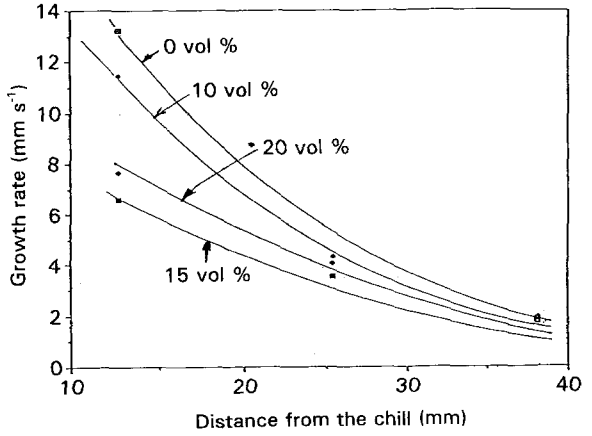

Figure 4 Influence of dispersion of silicon carbide in aluminium–silicon alloy on the macroscopic growth rate of the solidification front at various distances from the chill.

3.5. Model analysis

Various models have been developed to predict whether a particle ahead of a planar growing solid–liquid interface will be captured or engulfed by the interface. All models are based on critical velocity of the dendrite tip during solidification. (We have attempted to analyse existing models, even though they were developed for planar front solidification, because there are no models available for the interaction between the dendritic solidification front and particles.)

According to Uhlmann *et al.*'s model, the critical velocity of a planar solid–liquid front for particle engulfment is given by [13]

$$V_{cr} = \frac{n+1}{2}\left(\frac{\Delta H_f \rho a_o V_o D}{KTR^2}\right) \quad (1)$$

where R is the radius of the particulate, D, a_o and V_o are the diffusion coefficient, lattice constant and atomic volume of solidifying material, respectively, $n = 5.0$ [13], K is the Boltzmann constant and T is the temperature.

Bolling and Cisse [14] have proposed a model based on the viscous drag of a liquid on a particulate during solidification. According to them, the critical velocity for particle engulfment ahead of a planar interface is

$$V_{cr} = \left[\frac{4\psi(\alpha) KT \sigma_{sl} a_o}{9\pi \eta^2 R^3}\right]^{1/2} \quad (2)$$

where η is the viscosity of the liquid, σ_{sl} is the solid–liquid interface energy, and $\psi(\alpha)$ is a constant 0.34 [14]. Chernove *et al.* [15] have proposed a model based on the chemical potential criterion. According to them, the critical velocity for engulfment of particles is given by

$$V_{cr} = \frac{0.14 B_3}{\eta R}\left[\frac{\alpha}{B_3 r}\right]^{1/3} \quad (3)$$

where B_3 (10^{-21} J) and α (0.1) are constant [15]. The authors have considered forces of molecular interactions in a particulate molten film crystal system, when the gap between the particulate and the solidifying phase is less than 10^{-5}–10^{-6} cm (100–10 nm).

Stefanescu *et al.* [16] have considered the effects derived from differences in thermal conductivity between particulate and solidifying phase, and have used force balance at the particle in front of the solid–liquid interface to derive critical velocity [16].

$$V_{cr} = \frac{\Delta \sigma_o a_o}{6(n-1)\eta R}\left[2 - \frac{K_p}{K_L}\right] \quad (4)$$

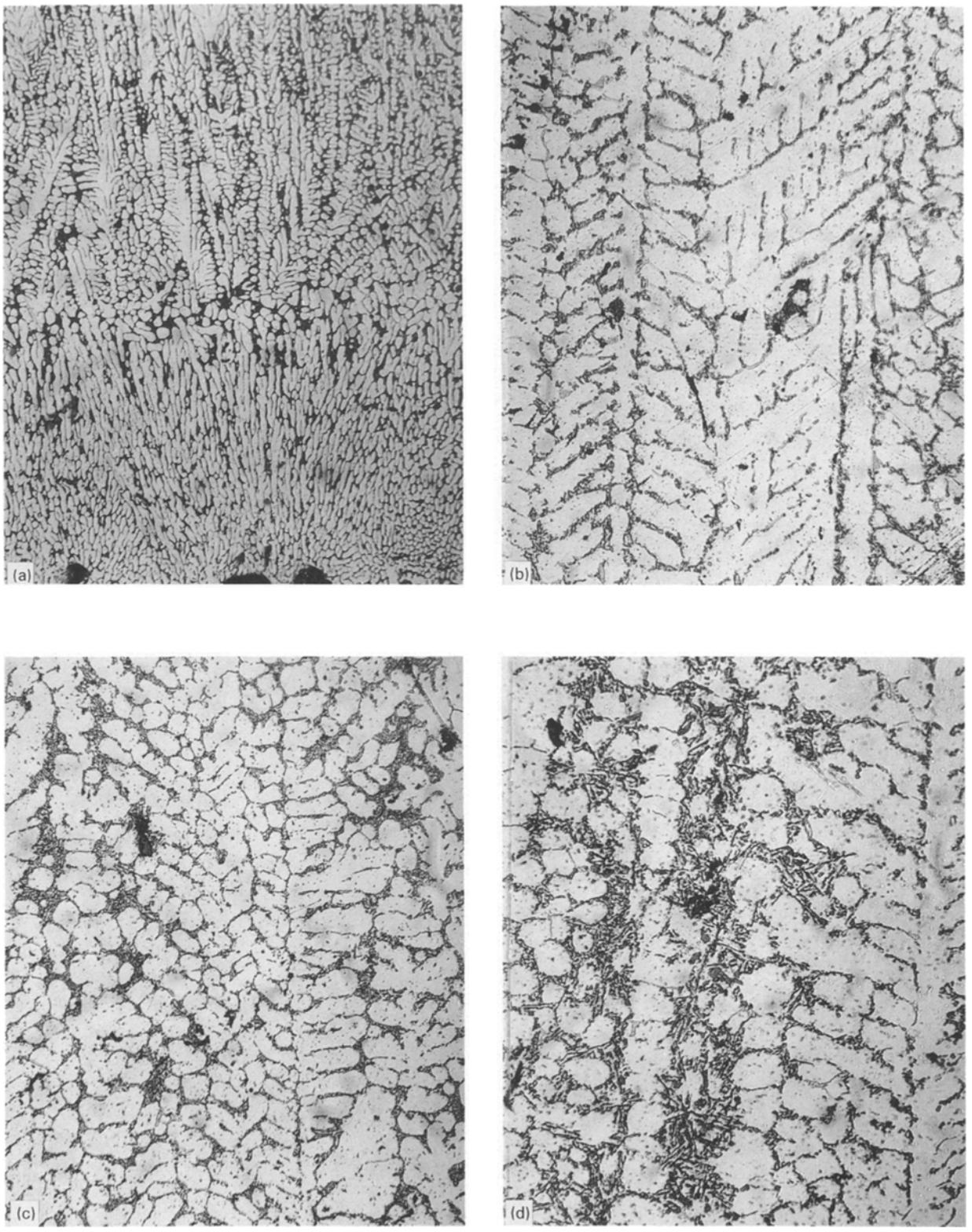

Figure 5 Microstructure of directionally solidified aluminium–silicon alloy containing 0 vol % SiC at various distances from the chill. (a) Chill zone, (b) 24 mm, (c) 40 mm, (d) 50 mm × 148.

where $\Delta\sigma_o$ is the surface energy difference between particulates and the solidification phase, n is a constant (7.0), and K_p and K_L are thermal conductivity of particulates and the solidifying phase, respectively.

Surappa and Rohatgi [17] have proposed a model based on thermal diffusivity ratio of particle and melt. According to them [17], the criterion for particle engulfment is

$$\left(\frac{\lambda_1 C_1 \rho_1}{\lambda_2 C_2 \rho_2}\right)^{1/2} \quad (5)$$

where λ, C and ρ have the normal nomenclature. The critical velocities for particle engulfment have been

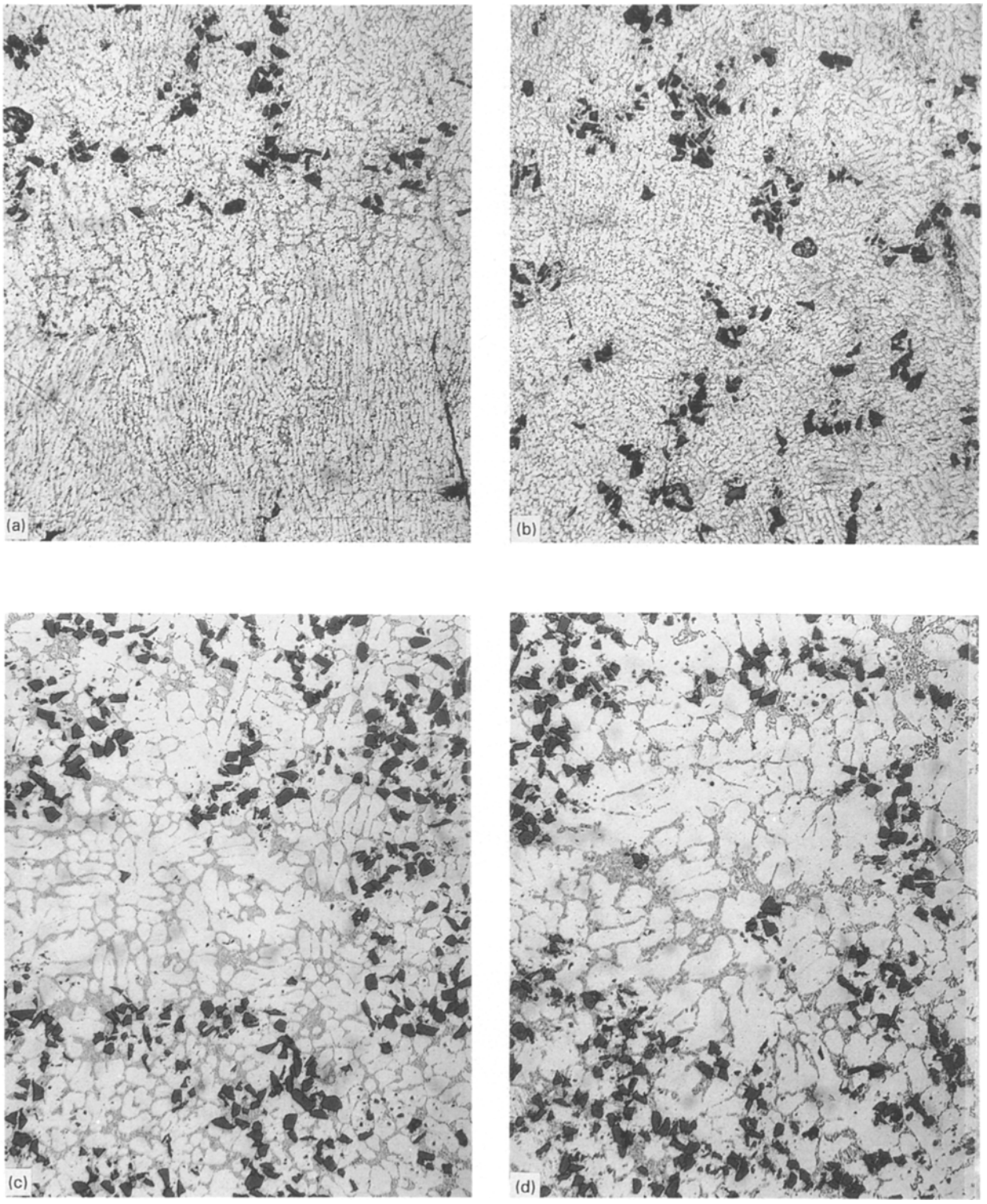

Figure 6 Microstructure of directionally solidified aluminium–silicon alloy containing 20 vol % SiC at various distances from the chill. (a) Chill zone, (b) 10 mm, (c) 12 mm, (d) 24 mm × 148.

calculated for different conditions and are shown in Table II.

In the present investigation, the actual velocities of growth of solid–liquid interface in the presence of various volume fractions of SiC is estimated by calculating local solidification time using the following equations:

$$\text{local solidification time, } t_f = \frac{T_l - T_s}{\text{cooling rate}} \quad (6)$$

$$\text{interface velocity} = \frac{\text{DAS}}{2t_f} \quad (7)$$

The estimated values of local solidification time and critical velocity are given in Table III and Fig. 7 shows variation of estimated interface velocity as function of cooling rate, for various volume fractions of silicon carbide. It is evident from the figure that interface velocity increases with increasing cooling rate for both the base alloy as well as the composites. Alloys containing 10 and 15 vol % SiC show somewhat

TABLE II Predictive equations for engulfment of primary α-aluminium phase on particles in terms of critical velocity

Model	Criteria for pushing	Calculated results for Al–SiC
Uhlmann *et al.* [13]	$V_{front} < V_{cr}$; $V_{cr} = \frac{(n+1)}{2}\left[\frac{\Delta H_f \rho a_o D}{KTR^2}\right]$	$V_{cr} = 0.187\ \mu m\ s^{-1}$ for $R = 10\ \mu m$
Bolling and Cisse [14]	$V_{front} < V_{cr}$; $V_{cr} = \left[\frac{4\psi(\alpha) KT \sigma_{sl} a_o}{9\pi\eta^2 R^3}\right]^{1/2}$	$V_{cr} = 4.24\ \mu m\ s^{-1}$ for $R = 10\ \mu m$
Chernov *et al.* [15]	$V_{cr} = \frac{0.14B_3}{\eta R}\left[\frac{\alpha}{B_3 R}\right]^{1/3}; \frac{\lambda^2}{l} > R$	$V_{cr} = 1.959\ \mu m\ s^{-1}$ for $R = 10\ \mu m$
	$V_{cr} = \frac{0.15B_3}{\eta R l}; \frac{\eta^2}{l} < R$	$V_{cr} = 2.38\ \mu m\ s^{-1}$
Stefanescu *et al.* [16]	$V_{front} < V_{cr}$; $V_{cr} = \frac{\Delta\sigma_0 a_o}{6(n-1)\eta R}\left[2 - \frac{K_p}{K_L}\right]$	$V_{cr} = 3120\ \mu m\ s^{-1}$ $R = 10\ \mu m$ $V_{cr} = 2048\ \mu m\ s^{-1}$ $R = 25\ \mu m$ $V_{cr} = 512\ \mu m\ s^{-1}$ $R = 100\ \mu m$
Surappa and Rohatgi [17]	$\left[\frac{\lambda_1 C_1 \rho_1}{\lambda_1 C_1 \rho_1}\right]^{1/2} < 1$	$\left[\frac{\lambda_p C_\rho \rho_\rho}{\lambda_p C_1 \rho_1}\right]^{1/2} = 0.056$

TABLE III Estimated values of local solidification time and interface velocity

Distance from chill (mm)	Arm spacing (μm) for vol % SiC				Cooling rate[a] (°C s^{-1})	Local solidification time (s)	Interface velocity (μm s^{-1}) for vol % SiC			
	0	10	15	20			0	10	15	20
12.7	18	24	22	19	28	1.4	6.4	8.5	7.8	6.7
25.0	22	31	37	22	12.5	3.28	3.3	4.7	5.6	3.3
38.0	26	50	43	27	5.6	7.32	1.7	3.4	2.9	1.8
50.0	36	62	51	38	3.5	11.7	1.5	2.6	2.1	1.6

[a] Taken from Fig. 7.

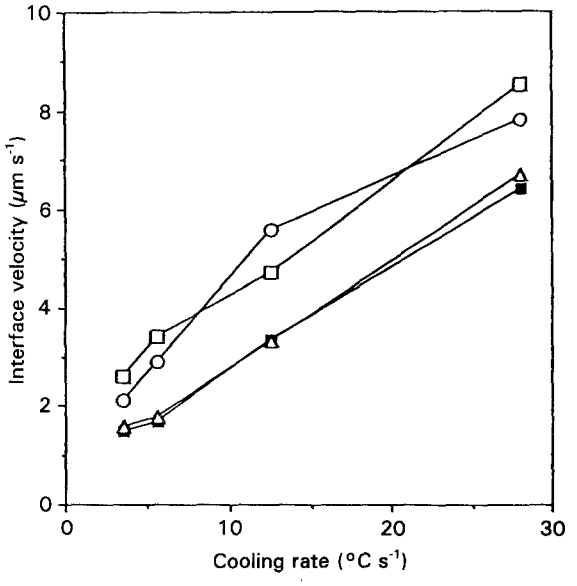

Figure 7 Variation in estimated interface velocity as a function of cooling rate. Vol % SiC: (■) 0, (□) 10, (○) 15, (△) 20.

higher interface velocities at any given cooling rate. In addition, an attempt was made to estimate critical interface velocity engulfment for different volume fractions of SiC. The theoretical critical velocities calculated for engulfment from different models and the estimated values of actual interface velocities of dendrites in the present experimental results are given in Tables II and III, respectively. It is apparent from the tables that models for particle engulfment, based on thermal properties (Stefanescu *et al.* [16] and Surappa and Rohatgi [17]) seem to agree with the experimental results (there is an order of magnitude difference in estimated critical velocity and the velocity calculated at a thermocouple nearest to the chill) of particle pushing observed in the present study for aluminium–silicon alloy containing SiC particles. The other models predict engulfment of the particles under the conditions of the present study, whereas in fact pushing of the particles by growing α-dendrites is observed. However, it is to be noted that each model cited in this paper makes various assumptions which may be at variance with the present study; in addition, there can be large variations in values of critical parameters such as interfacial and surface energies. The proposed models have been developed for a planar interface, whereas in the present experiments the solidification front was dendritic; this may be an additional reason for disagreement between the proposed theories and experiments.

In the region near the chill, average dendrite arm spacing is somewhat smaller than the average particle

size. Lloyd [11] has suggested that, under the cooling conditions, where the dendrite spacing is much smaller than the interparticle spacing, the distribution of the particles may remain closer to what existed in the liquid prior to solidification. However, during directional solidification, in the region (Fig. 6a) close to the chill, the vertically growing, closely spaced cells have macroscopically pushed the silicon carbide particles upwards out of the region.

The particle distribution becomes relatively more homogeneous on a macroscopic scale at increasing distances from the chill when secondary arms have started to form. Also, a detailed analysis of microstructures at various distances from the chill, as shown in Fig. 6c and d, indicates that the presence of SiC particles disrupts the orderly columnar structure generally observed in the base alloy. This may be attributed to the presence of particles disturbing the local temperature fields in the molten slurry. In addition, there is some evidence of dendrites terminating at a particle. In certain locations, splitting of a dendrite by a particle is also observed; this type of dendrite splitting has been noted earlier by Sekhar and Trivedi [18]. Both these effects are likely to alter the dendrite arm spacing compared with what is observed in the unreinforced alloy.

Fig. 8 shows the variation in average secondary dendrite arm spacing with distance from the chill. The average dendrite arm spacing generally increases linearly with increasing distance from the chill, for the base alloy and the composites. The dendrite arm spacings of the base alloy and the composites are similar up to about 25 mm from the chill. At a distance greater than 25 mm, the dendrite arm spacings are generally larger for the composites. The temperature profiles have shown that at distances greater than 25 mm from the chill, the temperature gradient and growth rate become very low. These lower values imply that the dendrite arm spacing is sensitive to the presence of silicon carbide particles under these conditions. It is interesting to note that the alloy containing 10 vol % SiC particles have the largest dendrite arm spacing, while the alloy containing 20 vol % particles and the base alloy have lower dendrite arm spacings. The analysis of microstructures indicates that the presence of particles in the alloy melt may have played two contradictory roles: (1) the particles may reduce the cooling rate locally near the particles, resulting in an increase in the dendrite arm spacing, and (2) they may split the dendrite arms and decrease the spacing. It is presumed that in alloys containing a lower volume fraction of particles (10%), trend 1 may dominate, while in alloys containing higher volume fraction of particles (15% and 20%), trend 2 may be dominating. However, the presence of particles does not appear to have a significant influence on dendrite arm spacings at a distance less than 20 mm from the chill, where an average cooling rate higher than 11 $^{\circ}C s^{-1}$ may exist and the dendrite arms are more numerous.

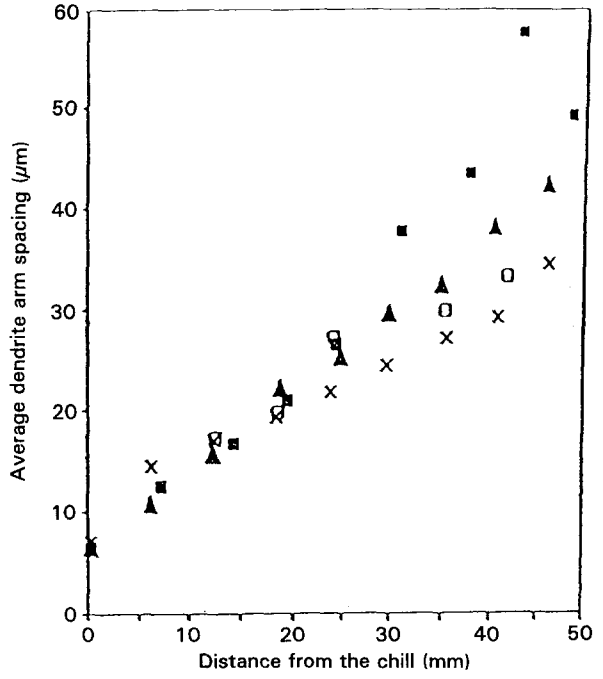

Figure 8 Variation in average dendrite arm spacing as a function of distance from the chill. (×) Monolithic alloy, (■) 10 vol % SiC, (△) 15 vol % SiC, (□) 20 vol %, SiC.

The change in dendrite arm spacing as a function of cooling rate for the base alloy and the composite is shown in Fig. 9. The cooling rate values are taken from the plot of cooling rate versus distance from the chill, as shown in Fig. 3. The cooling rates for both base alloys and the composites containing different volume fractions of SiC indicate that they are not significantly influenced by the presence of particles within the limits of our experimental measurements. Fig. 9 shows that the dendrite arm spacing decreases with increasing cooling rate by a power law relationship. It is interesting to note that the slope of the lines are similar for the base alloy as well as for the composites containing different volume fractions of SiC particles, although the DAS for the composite is higher. The relationship between the dendrite arm spacing (DAS) with cooling rate may be expressed by the following power law relationship for both the composites as well as the base alloy

$$\text{DAS} = b(\dot{T})^{-n} \tag{8}$$

where $\dot{T}$ is the cooling rate ($^{\circ}C s^{-1}$). The values of b and n for the composites containing different volume fractions of silicon carbide particles, including those for the base alloy are given in Table IV. The exponent n is observed to be about 0.33 and it appears to be a function of only the alloy chemistry. However, the coefficient b appears to be influenced by the presence of particles, and is higher for the composites, as illustrated in Fig. 10. It is noted that b is highest for the composite containing 10% particles, higher than the value observed with 20% particles. Additional studies are required to determine the role of particle volume per cent on the obstruction of growth of dendrite arms and the splitting of dendrite arms, two opposite effects which compete to produce the observed spacing. It is important to note that local solidification time and the shape of the cooling curve, profoundly influence the dendrite arm spacing and microsegregation [19, 20]. Sasikumar and Exner [19] have demonstrated

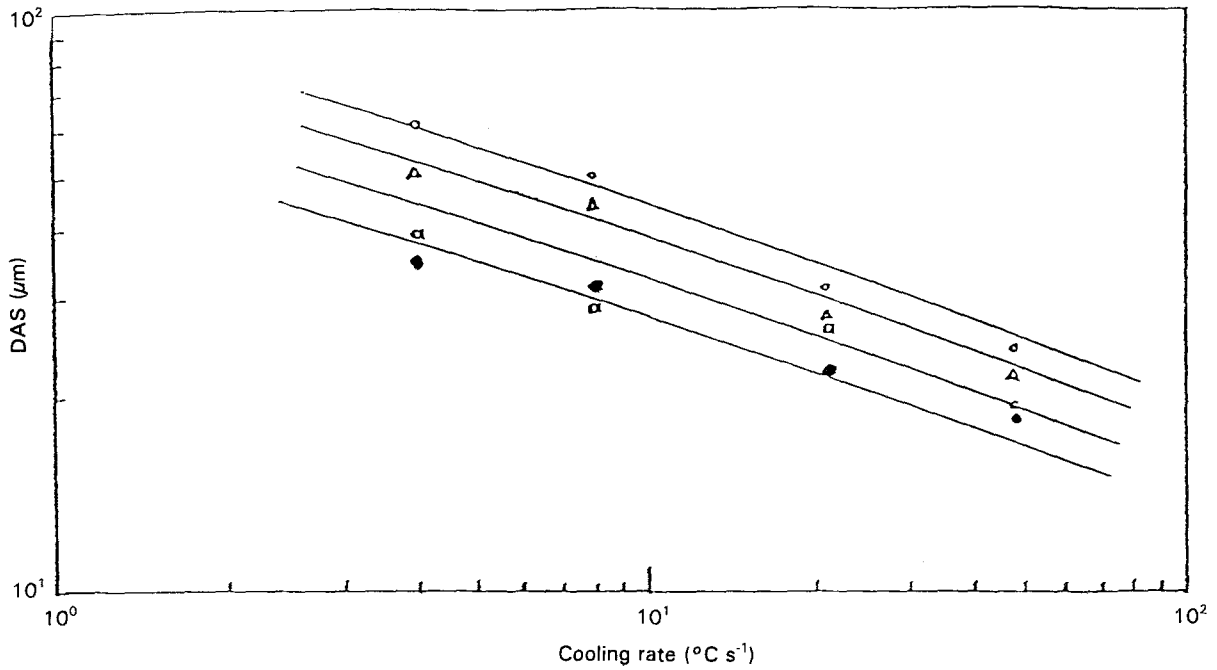

Figure 9 Variation in dendrite arm spacing as a function of cooling rate. Vol % SiC: (●) 0, (○) 10, (△) 15, (□) 20.

TABLE IV Values of constants b and n for monolithic alloys and alloys containing various volume fractions of silicon carbide particles

SiC (vol %)	b	Slope n
0	52	0.33
10	88	0.34
15	82	0.31
20	75	0.32

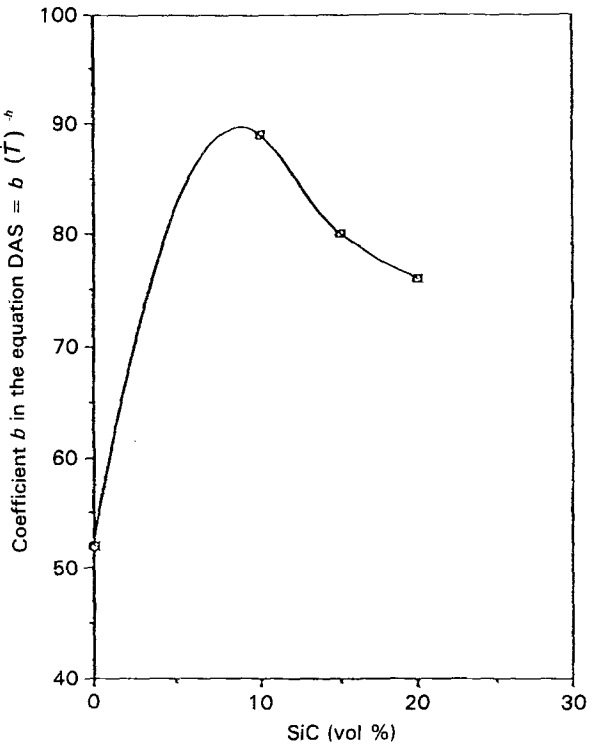

Figure 10 Coefficient b as a function of vol % SiC particles in aluminium–silicon alloy containing SiC particles.

through theoretical calculations of dendrite coarsening and microsegregation, that dendrite arm spacing and microsegregation may be significantly different for the same overall solidification time, with three extreme shapes of cooling curves. However, these calculations are available only for monolithic alloys. It is most likely that the presence of particles may significantly influence the process of dendrite coarsening and microsegregation.

4. Conclusions

Directional solidification experiments on Dural A-356 alloy containing SiC particles show that the presence of particles influences the growth orientation of dendrites and influences certain solidification parameters including temperature gradients, cooling rate and dendrite arm spacings. The experimental results indicate the following points.

1. A particle-free region was generally observed in the solidified composite adjacent to the copper chill, indicating that in spite of higher cooling rate conditions, particles are pushed vertically up by the array of closely spaced dendrites growing from the chill.

2. The presence of particles in the alloy changes the orderly growth of dendrites observed in the base alloy, and the silicon carbide particles segregate to the last freezing interdendrite regions.

3. Several existing models have been used to calculate the critical velocities at which the silicon carbide particles should be entrapped instead of being pushed. All the proposed models, except the two which take into account thermal diffusivity, predict entrapment of the particles under the conditions of the present study.

4. In addition to the microsegregation of particles in the interdendritic regions, there are particle-free zones in the cast regions which encompass several

dendrite arms frequently due to macrosegregation of particles in the melt.

5. The cooling rate decreases with distance from the chill for both the base alloy and composites, and the temperature gradients ahead of the solidification front are lower for the composites compared to the base alloy under identical thermal conditions.

6. A relationship of the form $DAS = b(\dot{T})^n$ was observed between dendrite arm spacing and the cooling rate for all the composites investigated. However, the coefficient was observed to be higher in the composites compared with base alloy.

Acknowledgements

The authors acknowledge the financial support of Office of Naval Research (Grant N00014-90J-4139, Monitor S. G. Fishman) and General Motors for conducting this investigation.

References

1. P. K. ROHATGI, *J. Metals* **43** (1991) 10.
2. M. K. AGHAJANIAN, J. T. BURKE, D. R. WHITE and A. S. NAGELBERG, *SAMPE Quarterly* **34** (1989) 817.
3. S. RAY, *Ind. J. Technol.* **28** (1990) 77.
4. O. KENNEDY, *Adv. Mater. Proc.* **6** (1991) 42.
5. P. K. ROHATGI, R. ASTHANA and S. DAS, *Int. Met. Rev.* **31** (1986) 115.
6. P. K. ROHATGI and R. ASTHANA, *J. Metals* **43** (1991) 35.
7. M. SKIBO, D. L. MORRIS and D. J. LLOYD, in "Proceedings of the Conference on Cast Reinforced Metal Composites", edited by S. G. Fishman and A. K. Dhingra (ASM, Metals Park, OH, 1988) p. 257.
8. M. A. BAYOUMI and M. SUERY, *ibid.*, p. 167.
9. M. SUERY and L. LAJOYE, in "Solidification of Metal Matrix Composites", edited by P. K. Rohatgi (TMS, Warrendale, PA, 1991) p. 171.
10. J. W. McCOY and F. E. WAWNER, "Proceedings of the Conference on Cast Reinforced Metal Composites", edited by S. G. Fishman and A. K. Dhingra (ASM, Metals Park, OH 1988) p. 237.
11. D. J. LLOYD, *Compos. Sci. Technol.* **35** (1989) p. 159.
12. Y. WU, H. LIU and E. J. LAVERNIA, in "Proceedings of the TMS Meeting", Chicago, edited by P. K. Rohatgi (TMS, Warrendale, PA, 1993) p. 41.
13. D. R. UHLMANN, B. CHALMERS and K. A. JACKSON, *J. Appl. Phys.* **35** (1964) 2986.
14. G. F. BOLLING and J. CISSE, *J. Cryst. Growth* **10** (1971) 56.
15. A. A. CHERNOV, D. E. TEMKIN and A. M. MELNIKOVA, *Sov. Phys. Crystallogr.* **21** (1976) 369.
16. D. M. STEFANESCU, B. K. DHINDAW, S. A. KACAR and A. MOITRA, *Metall. Trans.* **19A** (1988) 2847.
17. M. K. SURAPPA and P. K. ROHATGI, *J. Mater. Sci.* **16** (1981) 765.
18. J. SEKHAR, R. TRIVEDI and S. H. HAN, in "Solidification of Metal Matrix Composite", edited by P. K. Rohatgi (TMS, AIME, Warrendale, PA, 1990) p. 121.
19. R. SASIKUMAR and H. I. EXNER, *Scripta Metall.* (1992) submitted.
20. R. SASIKUMAR, personal discussion.

Received 9 September 1993
and accepted 21 March 1994